Published in final edited form as:
Calcif Tissue Int. 2005 May ; 76(5): 355–364. doi:10.1007/s00223-004-0111-3.

Quantification of Trabecular Bone Structure Using Magnetic Resonance Imaging at 3 Tesla—Calibration Studies Using Microcomputed Tomography as a Standard of Reference

C. A. Sell, **J. N. Masi**, **A. Burghardt**, **D. Newitt**, **T. M. Link**, and **S. Majumdar**
Musculoskeletal and Quantitative Imaging Research Group, Department of Radiology, University of California, San Francisco, Francisco, CA, USA

Abstract

The purpose of this study is to use high-resolution magnetic resonance (MR) imaging at 3 Tesla (3T) to quantify trabecular bone structure *in vitro* using femoral head specimens, and to correlate the calculated structure measures with those that were determined using microcomputed tomography (μCT), the standard of reference. Fifteen cylindrical cores were obtained from fresh femoral heads after total hip arthroplasty. MR images were obtained at 3T using a transmit–receive wrist coil. High-resolution coronal images were acquired using a modified three-dimensional (3D) fast-gradient echo sequence. From these data sets two-dimensional (2D) structural parameters analogous to bone histomorphometry were derived by using both mean intercept length (MIL) methods based on the plate model and the more recent model-assumption free 3D distance-transformation (DT) methods. The parameters measured by the 2D plate model-based MIL method and the DT method included apparent (App). BV/TV (bone volume/total volume), App. Tb.Th (trabecular thickness), App. Tb.Sp (trabecular separation), and App. Tb.N (trabecular number). Identical regions of interest were analyzed in the MR images and the μCT data sets, and similar structure measures were derived. The means and standard deviations of the parameters over all slices were calculated and MR-derived measures were correlated with those derived from the μCT data sets using linear regression analyses. Structure measures were overestimated with MRI, for example, the mean App. BV/TV was 0.45 for MRI and 0.20 for μCT, and the slope of the graph was 1.45. App. Tb.Th was overestimated by a factor of 1.9, whereas App. Tb.Sp was underestimated; Tb.N showed the smallest effect. Correlations between the individual parameters were excellent (App. BV/TV, r^2= 0.82; App. Tb.Sp, r^2 = 0.84; App. Tb.N, r^2 = 0.81), except for App. Tb.Th (r^2 = 0.67). The results of this study show that trabecular bone structure measures may be obtained using 3T MR imaging. These measures, although higher than the standard of reference, show a highly significant correlation with true structure measures obtained by μCT.

Keywords

Trabecular bone structure; Magnetic resonance imaging; high resolution; Microcomputed tomography; Bone histomorphometry

Osteoporosis is a metabolic bone disorder defined as a disease associated with a reduction in bone mass and a deterioration of bone structure, both resulting in an increased bone fragility and susceptibility to fracture [1]. Amo re recent National Institutes of Health (NH) consensus statement [2] characterized osteoporosis as a disorder with compromised bone strength

Correspondence to: T. M. Link; tmlink@radiology.ucsf.edu.

resulting in an increased risk of fracture. In this statement, in addition to bone mass, bone quality was introduced referring to architecture, turnover, damage accumulation (e.g., microfractures), and mineralization.

For the clinical assessment of osteoporosis, X-ray–based methods such as dual X-ray absorptiometry (DXA) still remain the modality of choice for assessing bone mineral density. However, there is considerable overlap in the measured bone density values between fracture and nonfracture subjects. In the context of osteoporotic therapies, the reduction in fracture risk produced by some agents has not been entirely explained by increases in bone mineral density; for relatively small increases in bone density, much larger reductions in fracture risk have been demonstrated [3–7]. It is in this context, that there is a concerted effort to understand the role of bone quality, and as one of its components, the role of trabecular bone microarchitecture in defining bone strength. Initial studies have indicated that trabecular microarchitecture may be a particularly important determinant of bone strength [8–10], and increased attention is being directed to the *in vivo* assessment of trabecular bone microarchitecture.

Depiction of trabecular microarchitecture has progressed from destructive and sampling error-prone histomorphometry [11] to noninvasive, nondestructive imaging. Microcomputed tomography (μCT) has been demonstrated to be an excellent approach to the characterization of trabecular structure *in vitro* and *in vivo* [12–23]. Magnetic resonance imaging (MRI) has also seen success in both *in vitro* and *in vivo* depiction and quantification of trabecular structure [24–29]. With the goal of human, *in vivo* applications, the advantages of multi–planar capability, absence of ionizing radiation, continuously improving spatial resolution, and excellent contrast between bone and marrow makes MRI one of the most promising imaging techniques available for the characterization of trabecular bone microarchitecture.

The need to translate MR images into meaningful data for the quantification of trabecular structure has led to the development of a number of different approaches to image analysis and image processing. An example of the many measures derived from these approaches is a set of structural parameters analogous to standard histomorphometry [11,30,31], including bone volume fraction, trabecular thickness, trabecular spacing, and trabecular number. These structural indices have been evaluated and used in multiple calibration and validation studies, where they have been compared to information derived from other relevant modalities such as μCT, contact radiography of macrosections, and DXA[29,32–37]. A recent example of an approach used for image analysis is the application of distance transformation (DT) technique to MR images to derive structural parameters without assumption of any structural model [38]. Laib et al. reported good correlations between the new indices and those derived from the higher resolution μCT images [39]. Later application of the distance transformation (DT) method to MR images of the distal radius in postmenopausal women showed that measures obtained with this technique were comparable to spine or radius bone mineral density (BMD) measures in discrimination of fracture from nonfracture patients [40].

MR images *in vivo* are limited by the achievable signal-to-noise-ratio and thus the image quality. The tradeoff between total imaging time, image resolution, and image quality has limited the *in vivo* resolution to ~100 to 150 μm in-plane and between 300 and 1,000 μm in slice thickness. The size of individual trabeculae (80 to 150 μm) is on the same order as the resolution achieved with current scanning systems and as a result, partial volume blurring occurs. Because of this limited resolution, MR images reflect thicker trabeculae, and often thinner trabeculae are lost, or have partial-volume-induced thickening [41,42]. Other limitations arise with the use of gradient echo pulse sequences, most often used in imaging of trabecular bone. Artifacts resulting from differences in magnetic susceptibility of bone and marrow become apparent with this sequence, potentially affecting accuracy during analysis [41].

NR and thus image quality improves as a function of the field strength; therefore, it is expected that at higher field strength, such as at 3 Tesla (3T), the image quality for a fixed total scan time and resolution will improve. Alternatively, it may be possible to either obtain images with improved spatial resolution or to decrease the scan time needed to acquire quality images. In the context of trabecular bone imaging *in vivo*, both of these benefits promise to improve our existing capability to quantify structure. However, along with this improvement, other issues such as increased susceptibility effects at higher fields may play an important role in the quantitative assessment of trabecular structure. The goal of this study is to obtain quantitative measures of trabecular bone structure from MR images at 3T, and compare these measures to those obtained using μCT, as a standard of reference, and establish the calibration factors for high-field 3T assessment of trabecular bone structure.

Patients and Methods

Specimen Preparation

Fifteen cylindrical cores were obtained from the femoral heads of two patients who had undergone total hip arthroplasty for degenerative osteoarthritis of the hip. The patients who donated these specimens were 67- and 76-year-old men without other documented bone disease. The studies were performed in accordance with the rules and regulations of the institutional committee on research at the University of California, San Francisco.

The tissues were fixed in a formalin solution for storage before and after preparation. The cores were obtained with a 7.75-mm inner diameter diamond-tipped coring drill bit mounted on a drill press. The resulting cores ranged from 6 mm to 30 mm in length. A diameter of 7.75 mm allowed the cores to be mounted in the μCT machine and imaged at the desired resolution. In addition, this diameter allowed for adequate preparation for MR imaging.

In preparation for scanning, each core was defatted, degassed, and mounted in a customized container. Defatting of the cores involved placing the cores in scintillation vials where they were immersed in a 10% solution of an enzyme-active powdered detergent. The vials were placed in an ultrasonic cleaner and sonically agitated for 90-minutes. Vials were filled with new detergent solution, and additional cycles in the ultrasonic cleaner were performed until adequate removal of tissue had been achieved.

The cores were mounted in an array on three, thin acrylic plates using cyanoacrylate applied to the outer aspect of the cortical shell. The outer surface of the cortical shell was placed down on the plate so that the axis of each core was perpendicular to the surface of the plate. Each of the plates was then fixed into the bottom of a watertight plastic cube sized to fit into the wrist coil to be used for imaging. The cores were then immersed in 0.5 volume-% gadopentetate doped water to simulate the contrast found between yellow marrow and trabecular bone.

The cores were degassed prior to imaging to reduce artifacts arising from differences in susceptibility among air, solvent, and bone. The containers were placed in series with a vacuum pump, and eight cycles of 1 hour each were performed with intermittent manual agitation of the boxes to eliminate as much air as possible. The orientation of the cores with the cortical shell down minimized trapping of air as it moved toward the surface.

Magnetic Resonance (MR) Imaging

MR images were obtained at 3T with a GE Signa imaging system (GE Medical Systems, Milwaukee, WI, USA) equipped with 4 Gauss/cm gradients, and a transmit–receive wrist coil (USA Instruments, Aurora, OH, USA). High-resolution images were obtained using three-dimensional (3D) fast gradient echo sequence (FGRE) with a 6-cm field of view (FOV) and a matrix thickness of 512 × 512 pixels resulting in an in plane spatial resolution of 117 × 117

m^2. A slice 300 μm was chosen. A partial-echo acquisition was used with a repetition time (TR) of 30.0 ms, an echo time (TE) of 5.0 ms, a flip angle of 20°, and a bandwidth of 15.6 kHz and two excitations. To complete the data acquisition in one imaging session and complete coverage of two box holders, the acquisition time for each scan was 27 minutes.

MR Image Analysis

All analyses were performed on SUN/SPARC workstations (Sun Microsystems, Mountain View, CA, USA) with in-house software written in interactive display language (Research Systems, Inc., Boulder, CO, USA). Segmentation of the images into a bone and marrow phase required definition of regions of interest (ROIs), determination of an appropriate threshold, and binarization of the signal into bone and marrow phases. In defining the ROI for each core, a circular boundary was placed over the cross-section on the coronal image. The distance between the interior aspect of the cortical shell and the beginning of the ROI was recorded to aid in accurate matching when ROIs were chosen for μCT. The ROI was extended over 10 consecutive slices to create a cylinder with a length of 3 mm (slice thickness, 0.3 mm). The range of slices was also selected such that susceptibility artifacts resulting from trapped air, if present, were avoided. The threshold was set using a dual-reference technique as described previously by Majumdar et al. [43] This required the definition of a marrow and cortical bone phase by placing two ROIs on corresponding areas of the MR image. By using the signal intensity values within the region selected for analysis—the marrow and cortical bone signal intensities selected by the dual reference—the algorithm computes a threshold for image segmentation into bone and marrow phases.

Analysis of the trabecular bone in the binarized image involved determining 2D structural parameters analogous to bone histomorphometry using both mean intercept length (MIL) methods based on the plate model [44] and the more recent model-assumption free 3D distance transformation (DT) methods [38,39]. The parameters measured by the 2D plate model–based MIL method and the DT method include apparent (App.) BV/TV (bone volume/total volume), App. Tb.Th (trabecular thickness), App. Tb.Sp (trabecular separation), and App. Tb.N (trabecular number). These measures are analogous to those obtained in standard histomorphometry as described by Parfitt et al. [31,45]; however, they are labeled “apparent” measures because of the much lower resolution of the images from which these values are derived.

Determination of apparent structural measures by the MIL method involves the extension of a set of parallel rays across the binarized image at a series of angles (θ). Determination of App. Tb.Th begins with counting the number of black (bone) and white (marrow) pixel interfaces that are encountered by a set of parallel rays at a given angle θ. This value is used to determine the MIL by taking the ratio of the total area of the black pixels in the ROI versus half the number of edges counted. The overall mean width of the black pixels (App. Tb.Th) is obtained by taking the average MIL for all angles. App. BV/TV is calculated by the total number of black pixels representing bone over the total number of pixels in the ROI. App. Tb.N represents the area fraction of bone pixels/App. Tb.Th. App. Tb.Sp is equal to (1/App. Tb.N)–App. Tb.Th.

Determination of App. Tb.Th and App. Tb.Sp by using the DT method is accomplished by filling either the bone and marrow phases of the binarized image with maximal spheres. The mean diameter of all of the spheres used to fill the bone phase corresponds to the App. Tb.Th. App. Tb.Sp corresponds to the mean diameter of spheres filling the marrow phase. App. Tb.N is taken as the inverse of the mean distances between the structural elements of a skeletonized version of the image.

Microcomputed Tomography Imaging and Analysis

The 7.75-mm diameter cylindrical cores were fitted into cylindrical plastic vials with a slightly higher inner diameter after being wrapped in foam to prevent movement. The offsets recorded from the MR image (for each specimen the distance between the interior aspect of the cortical shell and the beginning of the ROI) were used to prescribe the identical region of interest on the scout view generated by a commercial μCT system (μCT 20, Scanco Medical AG, Bassersdorf, Switzerland). This scanner was used to obtain high-resolution images of each specimen with a voxel size of 22 μm in each dimension.

Analysis of μCT images involved the application of a low pass Gaussian filter (width = 0.5, support = 1 or a kernel size of 3) to remove noise and binarization by using a single manually selected global threshold (in between the two peaks in the histogram, Fig. 3c), which was constant for the entire study. Structural parameters (BV/TV, Tb.Th, Tb.Sp, and Tb.N) were derived using the DT method described previously. In addition, the structure model index (SMI), a parameter describing the general shape of the structure, was calculated [46]. The theoretical SMI value for a perfect cylinder (rod) is 3, while a perfect plate is 0. MIL-based measures on trabecular bone structure were also derived.

Bone Mineral Density Measurements

Bone mineral density is often considered a necessity in bone studies, as it is a methodology that can be extended easily to the clinical realm. To document these measures of bone mineral density (BMD) and their correspondence to our high resolution studies, BMD was measured using a DXA(Lunar Piximus, GE/Lunar, Madison, USA). Analysis was performed using the software provided by the manufacturer.

Statistical Analysis

The means and standard deviations of the parameters over all slices were calculated. The correlation between the MR-derived measures and those derived from μCT were compared using linear regression. All statistical computations were processed using JMP software (SAS Institute Inc., Cary, NC, USA).

Results

Figs. 1–3 show representative images obtained from a subset of the samples. As seen from the figures, a wide range of trabecular structures are seen in the specimens, and from the cross-sectional images as well as the 3D reconstructions, it can be noted that 3T MR images clearly depict trabecular bone structure. Compared to the μCT image, the MR image obtained with a lower spatial resolution shows similar architecture but also demonstrates the impact of partial volume, with mild blurring of the trabecular bone and trabeculae that appear larger in diameter.

Table 1 presents the mean values and standard deviations of the structural parameters obtained for both μCT and MRI using a model-independent estimate of bone architecture (DT) and the plate model method (MIL). All the trabecular structure measures obtained with μCT showed significant ($P < 0.0001$) differences from the MR-derived ones. The average SMI calculated from the μCT images for the specimens is 1, indicating in general more plate-like characteristics in these specimens. As seen from the table, the ratio of the MR-derived measures to the μCT measures is 2.44 for App. BV/TV, 1.98 for App. Tb.Th, 0.62 for App. Tb.Sp, and closest to 1 (1.23) for App. Tb.N using the DT method. The ratios for the MIL-derived measures show a similar trend. Figure 4 depicts the plot of these parameters, and from the slope of the graph it can be seen that the slope of App. BV/TV determined from MR images versus μCT images is 1.43 times. The slope of the App. Tb.Th from the linear regression was 0.89, with a positive intercept. The intercept depicts the limit of the MR image resolution, and emphasizes that

thinner trabeculae may be undetected. Similarly, the slope of the App. Tb.Sp graph was 0.66 and the slope of the App. Tb.N graph was 0.84. The slope of the graphs for MIL-based methods showed similar trends; however, the slope of the App. Tb.N and App. Tb.Th graph was closest to 1. The correlations of the individual parameters between the modalities, seen in Table 1, were highly significant with correlations of up to $r^2 = 0.84$ for App. Tb.Sp. The lowest correlation was found for App. Tb.Th $r^2 = 0.67$), which is not unexpected given the spatial resolution with MRI. The results of analysis of images obtained assuming a plate model show that the correlations of the individual parameters between the modalities μCT and MR, however, were not as good as those found with the model-independent measures parameters.

Table 2 shows the correlation between BV/TV and the other structure measures. As seen in column 2–4 for μCT the correlations between BV/TV and Tb.N, Tb.Th, and Tb.Sp are lower for the DT method compared to the plate model–based MIL methods, indicating perhaps that the DT measures contain information independent from BV/TV. The differences between the MIL and DT correlation for the measures derived from MR images is not as marked.

Structure parameters were also correlated with BMD and significant correlations were found (Table 3). As expected the highest correlations with BMD were found for App. BV/TV, since this parameter is most similar to bone mass. The correlations for μCT were a little higher than those obtained for MRI. The correlations for the other structural measures were substantially lower; the correlations were similar for both μCT and MRI.

Discussion

The role of MRI in the quantification of trabecular bone micro architecture has been demonstrated over the last decade, and numerous calibration and validation studies have been undertaken in which MR-derived measures of structure are compared with measures derived from other modalities, such as histology, μCT, BMD, and with biomechanical parameters. In MR-derived visualization and quantitation of structure, one of the main issues arises from the fact that the spatial resolution of *in vivo* MR images is often comparable to the thickness of the trabecular bone itself. This gives rise to partial-volume effects in the image and the image may not depict very thin trabeculae or may represent an average or a projection of a few trabeculae. With the recognition that MR-derived measures are not identical to histologic dimensions, a major focus in the field has been using established measures to investigate the resolution-dependence of MR-based measures and then calibrating MR-derived measures of bone structure. Hipp et al. [47] have compared the morphologic analysis of specimens of bovine trabecular bone by using both 3D MR reconstruction ($92 \times 92 \times 92\ \mu m^3$) and 2D optical images ($23 \times 23\ \mu m$) of the six faces of the samples. With the recognition of the partial-volume effects in MRI and the fact that MR-derived trabecular bone structure may not be identical to high-resolution μCT or histologic images, the notion of “apparent” trabecular bone network was introduced [32]. Although the “apparent” network is not identical to the “true” histologic structure, the apparent measures highly correlated highly with “true” measures [32,48]. The effect of slice thickness on standard morphologic measurements has been investigated by Kothari et al. [48]. Vieth et al. [49] compared standard morphologic measurements of 30 calcaneus specimens using MR imaging ($195 \times 195\ \mu m^2$ in plane resolution and 300/900 μm slice thickness) and contact radiographs (digitized with 50×50 μm in-plane spatial resolution) of sections obtained from the same specimens. The results of this study show that MR-based measurements were correlated significantly with those obtained from digitized contact radiographs. However, partial-volume effects resulting from slice thickness as well as image post-processing (thresholding) had substantial impact on these correlations–the thicker the slice, the poorer the correlation.

We obtained, at 3T, high-resolution MR images of trabecular bone in human bone cores from the femur and calculated quantitative measures of architectural parameters. Model-independent evaluation techniques for MR images were compared to more traditional evaluation techniques. μCT scans of the same cubes with a much higher resolution of 22 μm were taken as the gold standard, and differences in the structural measures obtained from MRI and higher resolution μCT were established. The MRI scans were performed at resolutions that are reasonable for use *in vivo* with in-plane resolution of 117 μm and a 300-μm axial resolution. Care was taken to reproduce *in vivo* conditions, but because of longer T2 times of gadopentetate-doped saline and the absence of motion artifacts, a mildly better image quality may have been achieved.

The accuracy of a new model-independent morphologic measure, based on the DT technique has been investigated by Laib et al. [39] and compared to high-resolution μCT images ($34 \times 34 \times 34\ \mu m^3$), and good correlation was found between the two sets of measurements, with the best $R^2 = 0.91$ for Tb.N.

By using a standardized thresholding criterion for all images Majumdar et al. [32] found an overestimation of trabecular bone area fraction (approximately 3 times), trabecular width (approximately 3 times), and an underestimation of trabecular spacing (approximately 1.6 times) in 1.5T MR images using 18-μm synchrotron-based μCT images as a gold standard. Since then, advances in MR imaging and reduced echo times have led to a reduction in this difference, and Laib et al. [39] found in radius specimens at 1.5T MR an overestimation of App. BV/TV and Tb.Th by a factor of 2, an underestimation of App. Tb.Sp by a factor of 0.86, and no substantial over- or underestimation of App. Tb.N. In this report, our results at 3T as shown in Table 1 are comparable in magnitude to those of Laib et al. [39] at 1.5T, with similarly high correlations between MR- and μCT-based measures. The results of our current study demonstrated that the model-independent indices such as Tb.N from the μCT and MR images show lower correlation with BV/TV, and potentially contain more BV/TV-independent information as shown by Laib et al. [39]. However, at the resolution of the MR images, the differences between the model-independent and MIL-based methods are reduced considerably.

In this preliminary study, our aim was to show the feasibility of depicting trabecular bone structure at 3T and to correlate bone structure measures obtained at 3T with μCT structure measures by using this as a standard of reference. Although MR imaging at 3T has a higher SNR and thus allows higher spatial resolutions, we also have to consider more pronounced artifacts, such as an increase in susceptibility artifacts. This may in addition to partial-volume effects have increased App. BV/TV and Tb.Th. Nevertheless, correlations with μCT-derived measures were highly significant. In this study we used a gradient echo sequence, which as shown previously shown (32), increases trabecular dimensions. To reduce this effect, spin echo sequences have been applied [26,27]; however, these, have a lower SNR, and, thus, longer acquisition times are required to achieve comparable image quality. With the inherent higher SNR of imaging at 3T, however, these sequences may become more attractive. In addition to using different imaging sequences, the spatial resolution may also be increased given sufficient SNR. The feasibility of imaging trabecular bone at 3T has been demonstrated in this study but future work will have to focus on optimizing imaging sequences and spatial resolution.

Another issue would be the extension of MR imaging to other more central parts of the skeleton. Although MR imaging has shown good results both *in vivo* and *in vitro* in imaging calcaneus and distal radius MR imaging of the proximal femur *in vitro* at 1.5T has shown substantial limitations [50]. In this study, acquisition times to obtain sufficient SNR at 1.5T were not feasible *in vivo* and correlations between bone strength and structure measures were lower than those found between bone strength and BMD.

Limitations of this study have to be considered: We examined only a small sample of bone cores but since this was a feasibility study, larger studies are required to optimize imaging parameters and sequences. We also did not compare MR imaging at 1.5T and 3T directly, but extensive studies were performed at 1.5T in bone specimens and these data are available for comparison [39].

In conclusion this study shows that at 3T, the noninvasive determination of trabecular bone structure makes MR a promising tool in the quantitative assessment and monitoring of skeletal status. With the higher signal-to-noise-ratio, and improved image quality that is possible at higher fields, MR at 3T may play a significant role analyzing trabecular bone structure *in vivo* to understand metabolic bone disease and the response to therapy.

References

1. Consensus development conference: diagnosis, prophylaxis, and treatment of osteoporosis. Am J Med 1993;94:646–650. [PubMed: 8506892]
2. NIH consensus development panel on osteoporosis prevention, diagnosis, and therapy: March 7–29, 2000: highlights of the conferences. South Med J 2001;94:569–573. [PubMed: 11440324]
3. Black D, Cummings S, Karpt D, et al. Randomized trial of alendronate on risk of fracture in women with existing vertebral fractures. Lancet 1996;348:1535–1541. [PubMed: 8950879]
4. Ettinger B, Black DM, Mitlak BH, Knickerbocker RK, Nickelsen T, Genant HK, Christiansen C, Delmas PD, Zanchetta JR, Stakkestad J, Glüer CC, Krueger K, Cohen FJ, Eckert S, Ensrud KE, Avioli LV, Lips P, Cummings SR. Reduction of vertebral fracture risk in post-menopausal women with osteoporosis treated with raloxifene: results from a 3-year randomized clinical trial. Multiple Outcomes of Raloxifene Evaluation (MORE) Investigators [see comments]. JAMA 1999;282:637–645. [PubMed: 10517716]
5. Harris ST, Watts NB, Genant HK, McKeever CD, Hangartner T, Keller M, Chesnut CH 3rd, Brown J, Eriksen EF, Hoseyni MS, Axelrod DW, Miller PD. Effects of risedronate treatment on vertebral and nonvertebral fractures in women with postmenopausal osteoporosis: a randomized controlled trial. Vertebral Efficacy with Risedronate Therapy (VERT) Study Group. JAMA 1999;282:1344–1352. [PubMed: 10527181]
6. Chesnut CH 3rd, Silverman S, Andriano K, Genant H, Gimona A, Harris S, Kiel D, LeBo M, Maricic M, Miller P, Moniz C, Peacock M, Richardson P, Watts N, Baylink D. Arandomized trial of nasal spray salmon calcitonin in postmenopausal women with established osteoporosis: the prevent recurrence of osteoporotic fractures study. PROOF Study Group. Am J Med 2000;109:267–276. [PubMed: 10996576]
7. Sarkar S, Mitlak BH, Wang M, et al. Relationships between bone mineral density and incident vertebral fracture risk with raloxifene therapy. J Bone Miner Res 2002;17:1–10. [PubMed: 11771654]
8. Siffert RS, Luo GM, Cowin SC, Kaufman JJ. Dynamic relationships of trabecular bone density, architecture, and strength in a computational model of osteopenia. Bone 1996;18:197–206. [PubMed: 8833215]
9. Majumdar S, Kothari M, Augat P, Newitt DC, Link TM, Lin JC, Lang T, Lu Y, Genant HK. High-resolution magnetic resonance imaging: three-dimensional trabecular bone architecture and biomechanical properties. Bone 1998;22:445–454. [PubMed: 9600777]
10. Ulrich D, van Rietbergen B, Laib A, Reuegsegger P. The ability of three-dimensional structural indices to reflect mechanical aspects of trabecular bone. Bone 1999;25:55–60. [PubMed: 10423022]
11. Recker, RR. Bone histomorphometry: techniques and interpretation. CRC Press; Boca Raton, FL: 1983.
12. Reugsegger P, Koller B, Muller R. A microtomographic system for the nondestructive evaluation of bone architecture. Calcif Tissue Int 1996;58:24–29. [PubMed: 8825235]
13. Ulrich D, Van Rietbergen B, Laib A, Ruegsegger P. The ability of three-dimensional structural indices to reflect mechanical aspects of trabecular bone. Bone 1999;25:55–60. [PubMed: 10423022]

14. Müller R, Koller B, Hildebrand T, Laib A, Gianolini S, Rüegsegger P. Resolution dependency of micro-structural properties of cancellous bone based on three-dimensional mu-tomography. Technol Health Care 1996;4:113–119. [PubMed: 8773313]
15. Patel V, Issever AS, Burghardt A, Laib A, Ries M, Majumdar S. MicroCT Evaluation of normal and osteoarthritic bone structure in human knee specimens. J Orthop Res 2003;21:6–13. [PubMed: 12507574]
16. Laib A, Barou O, Vico L, Lafage-Proust MH, Alexandre C, Rügsegger P. 3D micro-computed tomography of trabecular and cortical bone architecture with application to a rat model of immobilisation osteoporosis. Med Biol Eng Comput 2000;38:326–332. [PubMed: 10912350]
17. Laib A, Ruegsegger P. Calibration of trabecular bone structure measurements of an in vivo 3D-QCT with a 28 μm microCT. Bone 1999;24:35–39. [PubMed: 9916782]
18. Laib A, Rüegsegger P. Calibration of trabecular bone structure measurements of in vivo three-dimensional peripheral quantitative computed tomography with 28-micron-resolution microcomputed tomography. Bone 1999;24:35–39. [PubMed: 9916782]
19. Laib A, Hauselmann HJ, Ruegsegger P. In vivo high resolution 3D-QCT of the human forearm. Technol Health Care 1998;6:329–339. [PubMed: 10100936]
20. Kuhn JL, Goldstein SA, Feldkamp LA, et al. Evaluation of a microcomputed tomography system to study trabecular bone structure. J Orthop Res 1990;8:833–842. [PubMed: 2213340]
21. Dufresne T. Segmentation techniques for analysis of bone by three-dimensional computed tomographic imaging. Technol Health Care 1998;6:351–359. [PubMed: 10100938]
22. Barou O, Valentin D, Vico L, Tirode C, Barbier A, Alexandre C, Lafage-Proust MH. High-resolution three-dimensional micro-computed tomography detects bone loss and changes in trabecular architecture early: comparison with DEXA and bone histomorphometry in a rat model of disuse osteoporosis. Invest Radiol 2002;37:40–46. [PubMed: 11753153]
23. Halloran BP, Ferguson VL, Simske SJ, Burghardt A, Venton LL, Majumdar S. Changes in bone structure and mass with advancing age in the male C57BL/6J mouse. J Bone Miner Res 2002;17:1044–1050. [PubMed: 12054159]
24. Takahashi M, Wehrli FW, Wehrli SL, et al. Effect of prostaglandin and bisphosphonate on cancellous bone volume and structure in the avariectomized rat studied by quantiative 3D NMR microscopy. J Bone Miner Res 1999;14:680–689. [PubMed: 10320516]
25. Gordon CL, Webber CE, Christoforou N, Nahmias C. In vivo assessment of trabecular bone structure at the distal radius from high-resolution magnetic resonance images. Med Phys 1997;24:585–593. [PubMed: 9127312]
26. Ma J, Wehrli FW, Song HK. Fast 3D large-angle spin-echo imaging 3D FLASE. Magn Reson Med 1996;35:903–910. [PubMed: 8744019]
27. Chung HW, Wehrli FW, Williams JL, Wehrli SL. Three-dimensional nuclear magnetic resonance microimaging of trabecular bone. J Bone Miner Res 1995;10:1452–1461. [PubMed: 8686500]
28. Majumdar S, Newitt DC, Mathur A, Osman D, Gies A, Chiu E, Lots J, Kinney J, Genant H. Magnetic resonance imaging of trabecular bone structure at the distal radius: relationship with X-ray tomographic microscopy and biomechanics. Osteoporos Int 1996;6:376–385. [PubMed: 8931032]
29. Majumdar S, Link TM, Augat P, Lin JC, Newitt D, Lane NE, Genant HK. Trabecular bone architecture in the distal radius using magnetic resonance imaging in subjects with fractures of the proximal femur. Osteoporos Int 1999;10:231–239. [PubMed: 10525716]
30. Nelson DA, Kleerekoper M, Parfitt AM. Bone mass, skin color, and body size among black and white women. Bone Miner 1988;4:257–264. [PubMed: 3191283]
31. Parfitt AM, Drezner MK, Glorieux FH, et al. Bone histomorphometry: standardization of nomenclature, symbols and units: Report of the ASBMR histomorphometry nomenclature committee. J Bone Miner Res 1987;2:595–610. [PubMed: 3455637]
32. Majumdar S, Newitt D, Mathur A, Osman D, Gies A, Chiu E, Lotz J, Kinney J, Genant H. Magnetic resonance imaging of trabecular bone structure in the distal radius: relationship with X-ray tomographic microscopy and biomechanics. Osteoporos Int 1996;6:376–385. [PubMed: 8931032]
33. Majumdar S, Kothari M, Augat P, et al. High-resolution magnetic resonance imaging: Three-dimensional trabecular bone architecture and biomechanical properties. Bone 1998;22:445–454. [PubMed: 9600777]

34. Lin JC, Amling M, Newitt DC, Selby K, Srivastav SK, Delling G, Genant HK, Majumdar S. Heterogeneity of trabecular bone structure in the calcaneus using magnetic resonance imaging. Osteoporos Int 1998;8:16–24. [PubMed: 9692073]
35. Beuf, O.; Ghosh, S.; Newitt, DC.; Link, TM.; Steinbach, L.; Reis, M.; Lane, N.; Majumdar, S. Characterization of trabecular bone micro-architecture in the knee in osteoarthrosis using high-resolution MRI. Proceedings of the 8th Annual Meeting of the ISMRM; Denver, CO. 2000. p. 2135
36. Link T, Majumdar S, Augat P, et al. In vivo high resolution MRI of the calcaneus: differences in trabecular structure in osteoporosis patients. J Bone Miner Res 1998;13:1175–1182. [PubMed: 9661082]
37. Vieth V, Link T, Letter A, Persigehl T, Newitt D, Heindel W, Majumdar S. Does the trabecular bone structure depicted by high-resolution MRI of the calcaneus reflect the true bone structure? Inves Radiol 2001;36:210–217.
38. Hildebrand T, Ruegsegger P. Anew method for the model-independent assessment of thickness in three-dimensional images. J Microsc 1997;185:67–75.
39. Laib A, Beuf O, Issever A, Newitt DC, Majumdar S. Direct measures of trabecular bone architecture from MR images. Adv Exp Med Biol 2001;496:37–46. [PubMed: 11783624]
40. Laib A, Newitt DC, Lu Y, Majumdar S. New model-independent measures of trabecular bone structure applied to in vivo high-resolution MR images. Osteoporos Int 2002;13:130–136. [PubMed: 11905523]
41. Majumdar S, Newitt D, Jergas M, Gies A, Chiu E, Osman D, Keltner J, Keyak J, Genant H. Evaluation of technical factors affecting the quantification of trabecular bone structure using magnetic resonance imaging. Bone 1995;17:417–430. [PubMed: 8573417]
42. Kothari M, Keaveny TM, Lin JC, Newitt D, Genant H, Majumdar S. Impact of spatial resolution on the prediction of trabecular architecture parameters. Bone 1998;22:437–443. [PubMed: 9600776]
43. Majumdar S, Genant HK, Grampp S, Newitt DC, Truong VH, Lin JC, Mathur A. Correlation of trabecular bone structure with age, bone mineral density, and osteoporotic status: in vivo studies in the distal radius using high resolution magnetic resonance imaging. J Bone Miner Res 1997;12:111–118. [PubMed: 9240733]
44. Harrigan T, Mann R. Characterization of micro-structural anisotropy in orthotropic materials using a second rank tensor. J Mater Sci 1984;19:761–767.
45. Parfitt AM. Bone histomorphometry: standardization of nomenclature, symbols and units: summary of a proposed system. J Bone Miner Res 1988;4:1–5.
46. Hildebrand T, Ruegsegger P. Quantification of bone microarchitecture with the structure model index. Comput Methods Biomech Biomed Eng 1997;1:15–23.
47. Hipp JA, Jansujwicz A, Simmons CA, Snyder B. Trabecular bone morphology using micro-magnetic resonance imaging. J Bone Miner Res 1996;11:286–297. [PubMed: 8822353]
48. Kothari M, Chen T, Lin J, Newitt D, Majumdar S, Genant H. Three dimensional bone architecture assessment: impact of image resolution. Osteoporos Int 1997;7:289.
49. Vieth V, Link TM, Letter A, Persigehl T, Newitt D, Heindel W, Majumdar S. Does the trabecular bone structure depicted by high-resolution MRI of the calcaneus reflect the true bone structure? Invest Radiol 2001;36:210–217. [PubMed: 11283418]
50. Link TM, Vieth V, Langenberg R, Meier N, Lotter A, Newitt D, Majumdar S. Structure analysis of high resolution magnetic resonance imaging of the proximal femur: in vitro correlation with biomechanical strength and BMD. Calcif Tissue Int 2003;72:156–165. [PubMed: 12370799]

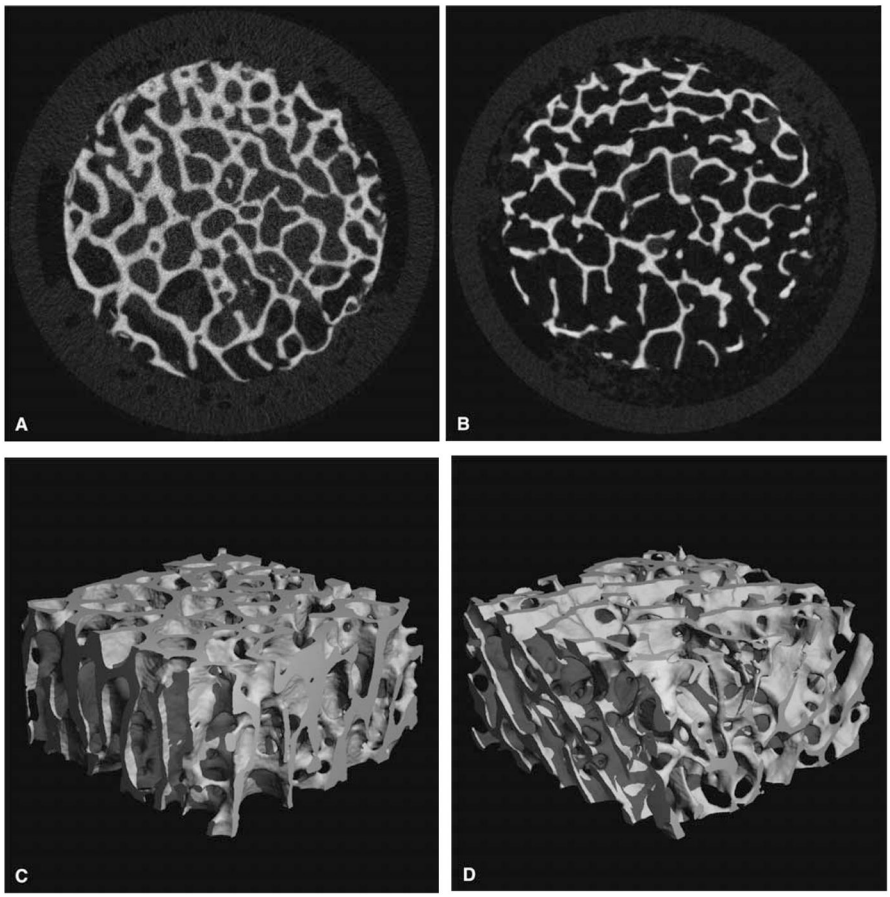

Fig. 1.

Representative cross-sectional images and three-dimensional (3D) renderings of the same bone specimen using microcomputed tomography (μCT) voxel size of 22 μm in each direction) (**A**) and (**C**) App. BV/TV = 0.32, (**B**) and (**D**) App. BV/TV = 0.19. App., apparent; BV/TV, bone volume/total volume.

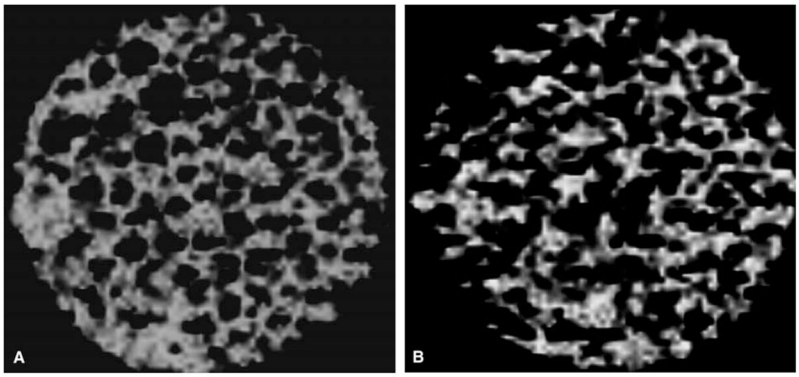

Fig. 2.

Magnetic resonance (MR) images with an in-plane resolution of 117 × 117 μm^2 of the same specimens shown in Fig. 1. (**A**) corresponds to specimen with MR-based App. BV/TV = 0.6, (**B**) App. BV/TV = 0.25. The images are shown in reverse gray scale, where bone is bright and the Gadopentetate solution is dark. App., apparent; BV/TV, bone volume/total volume.

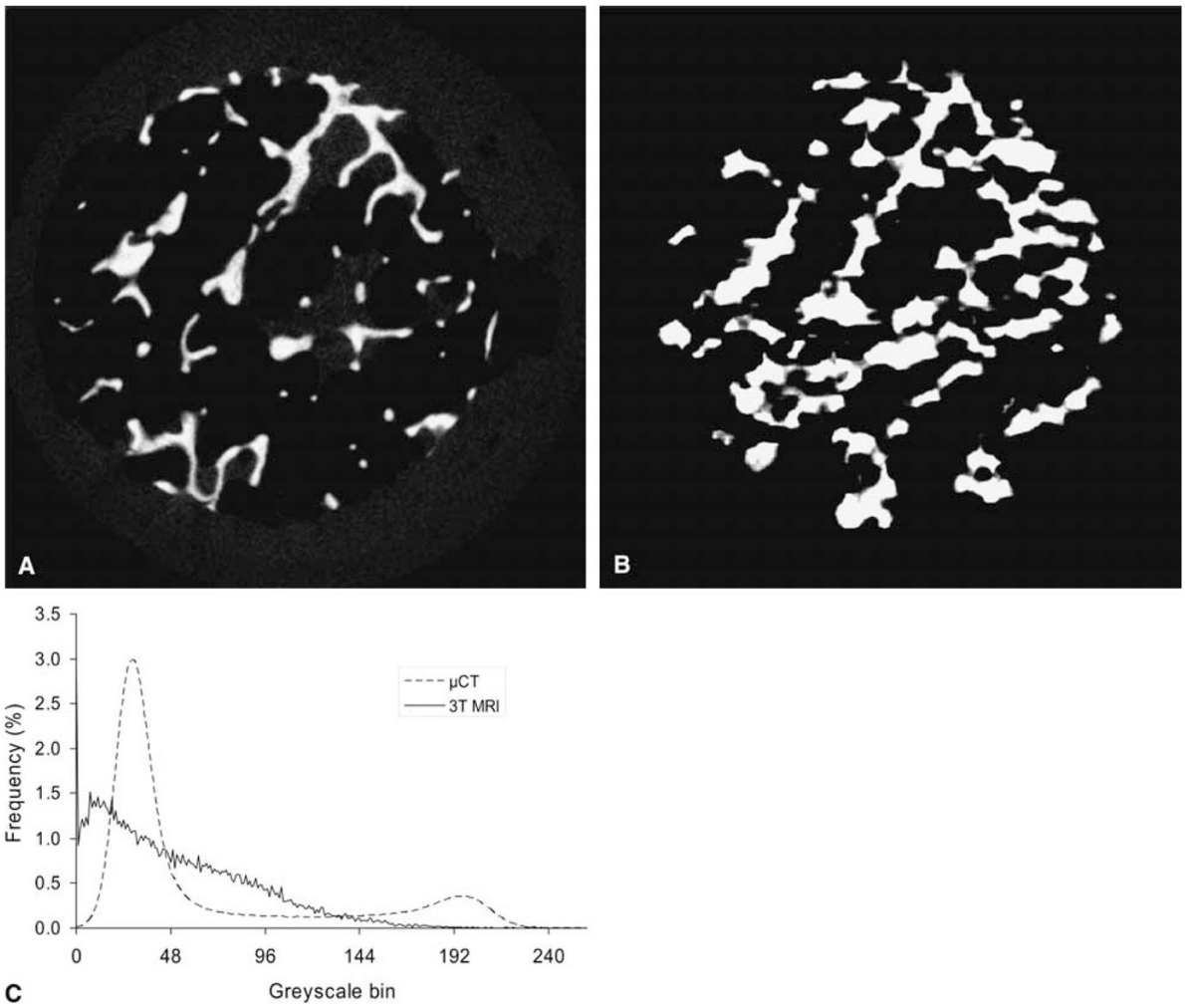

Fig. 3.

Matched slices as closely as possible for specimen shown in Figures 1B, D and Fig. 2B for visual comparison between microcomputed tomography (μCT) and magnetic resonance (MR) images. (**A**) μCT, (**B**) MR image, (**C**) representative intensity histograms are demonstrated showing a bimodal distribution for μCT and a single broad peak for MR.

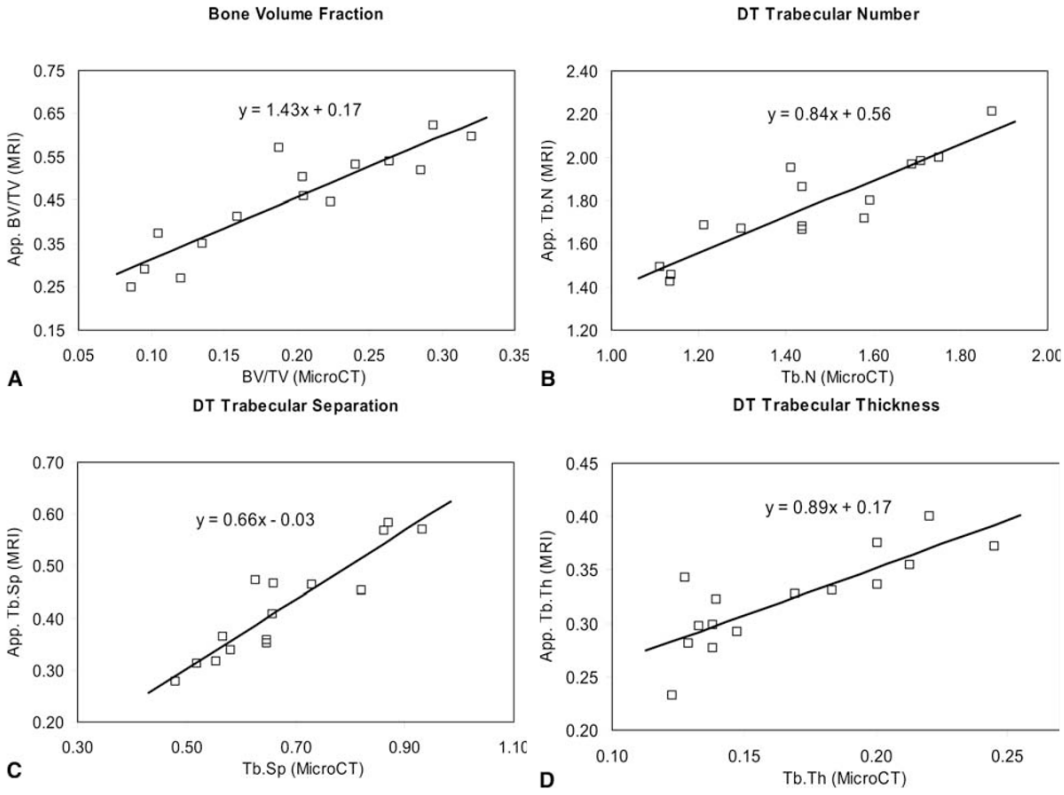

Fig. 4.

Plots showing the relationship between the magnetic resonance (MR)–derived measures and the microcomputed tomography (μCT) measures. Linear regression was used to obtain the correlation between the measures (*solid line*). The equation for the fit is shown on each plot.

Table 1

Mean value for all specimens of the structural indices derived using the model-independent distance transformation (DT) analysis of MR images, μCT images, and their ratios compared to similar parameters quantified using the mean intercept length (MIL) method

	Mean from μCT	Mean from DT MR	MR/μCT	Coefficient of determination (r^2)
BV/TV	0.195 ± 0.076	0.448 ± 0.120	2.44 ± 0.50	0.816
Tb.N.	1.454 ± 0.243	1.771 ± 0.226	1.23 ± 0.10	0.806
Tb.Th.	0.167 ± 0.040	0.323 ± 0.044	1.98 ± 0.30	0.665
Tb.Sp.	0.677 ± 0.138	0.421 ± 0.100	0.62 ± 0.06	0.840
SMI	1.00 ± 0.60			

	Mean from μCT (MIL)	Mean from 2D MR	MR/μCT	Coefficient of determination (r^2)
BV/TV	0.195	0.448	2.44 ± 0.50	0.816
Tb.N.	1.464 ± 0.336	1.836 ± 0.236	1.27 ± 0.10	0.774
Tb.Th.	0.131 ± 0.037	0.243 ± 0.052	1.66 ± 0.24	0.649
Tb.Sp.	0.588 ± 0.195	0.315 ± 0.113	0.46 ± 0.10	0.630

μCT, computed tomography; BV/TV, bone volume/total volume; Tb.N, trabecular number; Tb.Th, trabecular thickness; Tb.Sp, trabecular separation; MR, magnetic resonance.

The ratios of the MR-derived measures to the μCT measures were taken for each specimen and the average mean and standard deviation are presented. Linear regression between the MR-derived and μCT measures (plots shown in Fig. 4) was used to determine the correlation between the structural measures made using the two modalities. The coefficient of determination for the lines shown in Fig. 4 are presented. In addition, structure model index (SMI) and degree of anisotropy (DA) of the specimens were computed from the μCT images, and presented here to characterize the trabecular structure under study.

Table 2

Correlations (r) between the structure parameters obtained using the microcomputed tomography (μCT) and magnetic resonance (MR) images. The first column shows the correlation coefficient *r* between the mean intercept length (MIL)–derived measures, whereas column 2–4 represent the correlations between the measures made using the model-independent distance transformation (DT) method

μCT	**BV/TV**	**Tb.N**	**Tb.Sp**	**Tb.Th**
BV/TV	1	0.55	−0.57	0.81
Tb.N	0.76	1		
Tb.Sp	−0.88		1	
Tb.Th	0.89			1
MRI	**BV/TV**	**Tb.N**	**Tb.Sp**	**Tb.Th**
BV/TV	1	0.69	−0.82	0.74
Tb.N	0.65	1		
Tb.Sp	−0.93		1	
Tb.Th	0.86			1

μCT, microcomputed tomography; BV/TV, bone volume/total volume; Tb.N, trabecular number; Tb.Sp, trabecular separation; Tb.Th, trabecular thickness; MRI, magnetic resonance imaging

Table 3

Correlation (r) of structure parameters and bone mineral density (BMD) obtained by dual X-ray absorptiometry (DXA)

BMD versus	Correlation with μCT *r*	Correlation with MRI *r*
BV/TV	0.94	0.84
Tb. N	0.58	0.56
Tb. Th	0.72	0.59
Tb. Sp	−0.57	−0.66

μCT, microcomputed tomography; MR, magnetic resonance; BV/TV, bone volume/total volume; Tb.N, trabecular number; Tb.Th, trabecular thickness; Tb.Sp, trabecular separation